


Vibrational properties of graphene quantum dots: Effects of confinement, geometrical structure, and edge orientation

Dongxu Zheng, Peng Han ^{*}, Xinke Wang, Wenfeng Sun, Jiasheng Ye, and Yan Zhang

Department of Physics, Beijing Key Lab for Metamaterials and Devices, Capital Normal University, Beijing 100048, China



(Received 9 April 2021; revised 12 August 2021; accepted 13 August 2021; published 26 August 2021)

We perform *ab initio* density functional theory calculations to study the lattice vibrations of graphene quantum dots (GQDs) with triangular, quadrate, and hexagonal shapes in lateral confinement of 1 to 3 nm and terminated in both zigzag and armchair orientations. We see the vibrational properties of GQD transform from molecular type into bulk-like type with increasing dot size and the features of the vibrational density of state also highly depend on the symmetry of the GQD. We find that the out-of-plane vibrated standing waves induced by lateral confinement instead of the in-plane vibrations dominate the lattice vibrations of small GQDs. By projecting the vibrational eigenvectors of GQDs on those of single-layer graphene, we see the mixture of the out-of-plane and in-plane vibrational characters in GQDs as the result of the strong lateral confinement. We identify coherent acoustic phonon modes in GQDs and find that the size dependence of coherent acoustic phonon frequency increases with increasing the isotropy of nanostructures. Moreover, different confinement effects on lattice vibrations along zigzag and armchair edge orientations are identified from *ab initio* calculations. We describe the Raman intensity of GQDs and observe a blue shift of the G-mode position in GQDs comparing to that of the single-layer graphene. Combining the bond length distribution at the edge of GQDs with the positive Grüneisen parameters, we link such blue shift to the surface effect of GQDs.

DOI: [10.1103/PhysRevB.104.085430](https://doi.org/10.1103/PhysRevB.104.085430)

I. INTRODUCTION

The discovery of single-layer graphene (SLG) is one of the most important milestones of material science and it has fundamentally changed the landscape of many branches of science and technology over the past decades owing to the excellent physical properties of graphene with low toxicity and biocompatibility [1–6]. Although remarkable electron mobility as high as $15\,000\text{ cm}^{-2}\text{V}^{-1}\text{s}^{-1}$ enables graphene ideal for fabricating high-speed electronic devices, its gapless band structure restricts a variety of optical and optoelectronic applications [4,7–9]. To combine high-quality luminescence with graphene materials, Pan *et al.* synthesized blue luminescent graphene quantum dots (GQDs) by cutting graphene sheets into nanometer-sized pieces with well-confined shape via hydrothermal route in the early 2010s [10]. Following their pioneering work, enormous attention has been paid on GQDs. Till now, GQDs of circular, elliptical, triangular, quadrate, and hexagonal shapes with lateral dimension of a few to hundreds of nanometers have been well synthesized [11]. This renders GQDs not only as an attractive platform to study the basic principle of quantum effects [12,13] but also as a key component of the next-generation optoelectronic devices [11,14–19].

Importantly, a solid understanding of the electronic and vibrational properties is a decisive step for the future progress of GQD based optoelectronic devices. Indeed, the electrostatic confinement of Dirac Fermions in GQDs with the so-called

Klein paradox have been extensively studied in both theory and experiment [12,13,20–24]. On the other hand, despite a rather intense Raman spectrum studies have been focused on graphene flakes [25–29], studies on the vibrational properties of GQDs are still rare [30–32]. Unexpected effects from lateral confinement, edge orientation, and geometry structure on the vibrational properties of GQDs are to be unraveled. Moreover, in most of the theoretical studies where electron-phonon interaction, phonon-phonon interaction or other phonon-related process is considered, the lattice vibrations of GQDs were either calculated at the level of continuum models or roughly taken from the phonon states of SLG [32,33]. Systematic studies on the vibrational properties of GQDs are thus fundamentally important for both understanding the nature of lattice vibrations in 2D materials with lateral confinement and for further progress of the phonon-related process.

In this paper, we perform *ab initio* density functional theory (DFT) calculations to study the lattice vibrations of GQDs with lateral dimension of a few nanometers, which is typical in experiments [34,35]. To investigate the effects of edge orientation and geometry structure on the vibrational properties, we calculate the vibrational eigenmodes of GQDs with triangular, quadrate, and hexagonal shapes terminated by both zigzag and armchair edge structures. A schematic of GQDs studied in this paper is given in Fig. 1(a). As shown in Fig. 1(a), the size of GQD L , which is defined as the maximum distance between two carbon atoms in the quantum dot, is labeled on GQDs with different geometry and edge structures. To compare the vibrational density of state (DOS) of GQDs with that of SLG, we define a similarity function to measure the

^{*}hanpeng0523@163.com

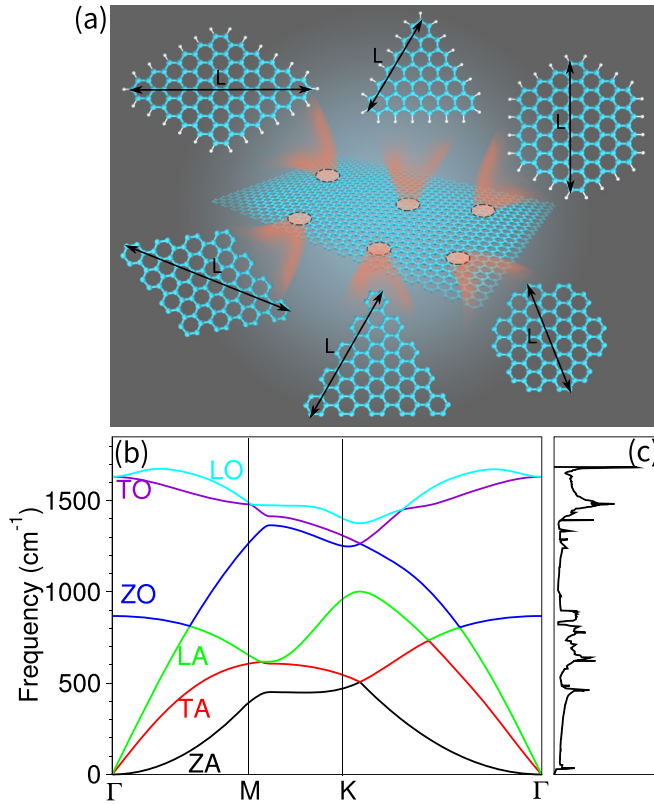


FIG. 1. (a) Schematic illustration of triangular, quadrate, and hexagonal shaped GQDs with zigzag and armchair edge structures. The size of GQD L , which is defined as the maximum distance between two carbon atoms in quantum dots, is labeled on the GQDs. (b) Phonon dispersion curve of SLG along high-symmetry axes. (c) Phonon DOS of SLG.

tendency to mimic the vibrations of SLG. From our *ab initio* calculation, we find that the vibrational properties of GQDs change from a form of molecular-like discrete type DOS to a SLG-like form with increasing dot size and high value of similarity is obtained for GQDs with the same point group symmetry as SLG. We find the out-of-plane vibrated standing waves induced by lateral confinement instead of the in-plane vibrated modes dominate the lattice vibrations of GQDs. By projecting the vibrational eigenvectors of GQDs on those of SLG, we see the characters of the out-of-plane vibrations are mixed with those of the in-plane modes in GQDs as the result of strong lateral confinement. We find stronger confinement effect on acoustic phonon modes than optical modes in GQDs and link this feature with continuum models. Moreover, we identify the vibrations of the coherent acoustic phonon modes in GQDs with various geometry structures and edge orientations. Strong size dependence of coherent acoustic phonon frequency is found in GQDs with high isotropy geometry structure. In addition, different confinement effects on the lattice vibrations of GQDs in the zigzag and armchair edge orientations are obtained from our DFT calculations. We also study the Raman intensity of GQDs and observe a blue shift of the G-mode position in GQDs compared to that of the SLG. Combining the bond length distribution at the edge of GQDs

with the positive Grüneisen parameters, we attribute the blue shift of the G-mode as the result of the surface effect in GQDs.

II. THEORETICAL METHOD

We constructed the GQDs by cutting a triangular, quadrate, or hexagonal graphene piece from a SLG flake along zigzag or armchair orientation at the edges. To avoid the surface states in zigzag edged GQDs, carbon atoms located at the zigzag edges with dangling bonds are terminated by hydrogen atoms. Due to the missing of C_3 and C_6 rotational symmetry and S_3 and S_6 improper rotational symmetry in triangular and quadrate structures, the point group symmetry decreases from D_{6h} (with 24 operations) of SLG to C_{2h} (with 4 operations) of triangular GQDs and D_{2h} (with 8 operations) of quadrate GQDs, respectively. The *ab initio* DFT calculations are performed using the local density approximation (LDA) and Trouiller-Martin normconserving pseudopotentials with an energy cutoff of 30 Ry. To avoid interaction between adjacent images, a vacuum of 10 Å is added between the outermost atoms. The equilibrium positions of atoms in GQDs are optimized until the forces are reduced to less than 3×10^{-6} Hartree/Bohr under constrained symmetry. The dynamical matrix elements are then calculated via finite difference approach with the optimized geometry structures. The vibrational frequencies ω along with the corresponding eigenmodes \mathbf{U} of GQDs are thereafter obtained via diagonalization of the dynamical matrix,

$$\sum_J \frac{1}{\sqrt{M_I M_J}} \frac{\partial^2 V(\mathbf{R})}{\partial \mathbf{R}_I \partial \mathbf{R}_J} \mathbf{U}_J = \omega^2 \mathbf{U}_I, \quad (1)$$

where $M_{I(J)}$ is the mass of atom $I(J)$, $V(\mathbf{R})$ denotes the potential energy surface as function of atomic position \mathbf{R} , and $\mathbf{R}_{I(J)}$ represents the position of atom $I(J)$, respectively [36–38]. All the DFT calculations of GQDs are performed using the CPMD code package [39].

In this paper, we define atoms, which only have two nearest neighboring carbon atoms, along with their nearest neighbors as edge atoms while the others are core atoms, respectively. In order to separate the contributions from the core and the edge atoms on the lattice vibrations, we calculate the projection coefficients,

$$\alpha_{c(e)}^v = \frac{\sum_I^{N_c(N_e)} |\mathbf{X}_I^v|^2}{\sum_{I=1}^N |\mathbf{X}_I^v|^2}, \quad (2)$$

with N_c , N_e , and N denoting the core, the edge, and the total number of atoms, respectively. The three-component vector \mathbf{X}_I^v represents the motion belonging to atom I from the $3N$ -component eigenvector \mathbf{U}^v with mode v [37,40]. To investigate the origin of lattice vibrations of GQDs from SLG, we project the vibrational eigenvectors of GQDs \mathbf{U}^v on the $3N$ -component vectors constructed by the phonon modes of SLG as

$$\mathbf{U}^v = \sum_{n,q} C_{n,q}^v \mathbf{U}_{n,q}^{\text{SLG}}. \quad (3)$$

Here, the $3N$ -component vector is constructed as $\mathbf{U}_{n,q}^{\text{SLG}} = \sum_I \mathbf{u}_{n,q}^\tau \exp(i\mathbf{q} \cdot \mathbf{R}_I)$ with $\mathbf{u}_{n,q}^\tau$ the three-component of SLG phonon eigenvector for atom τ , phonon branch n , and wave

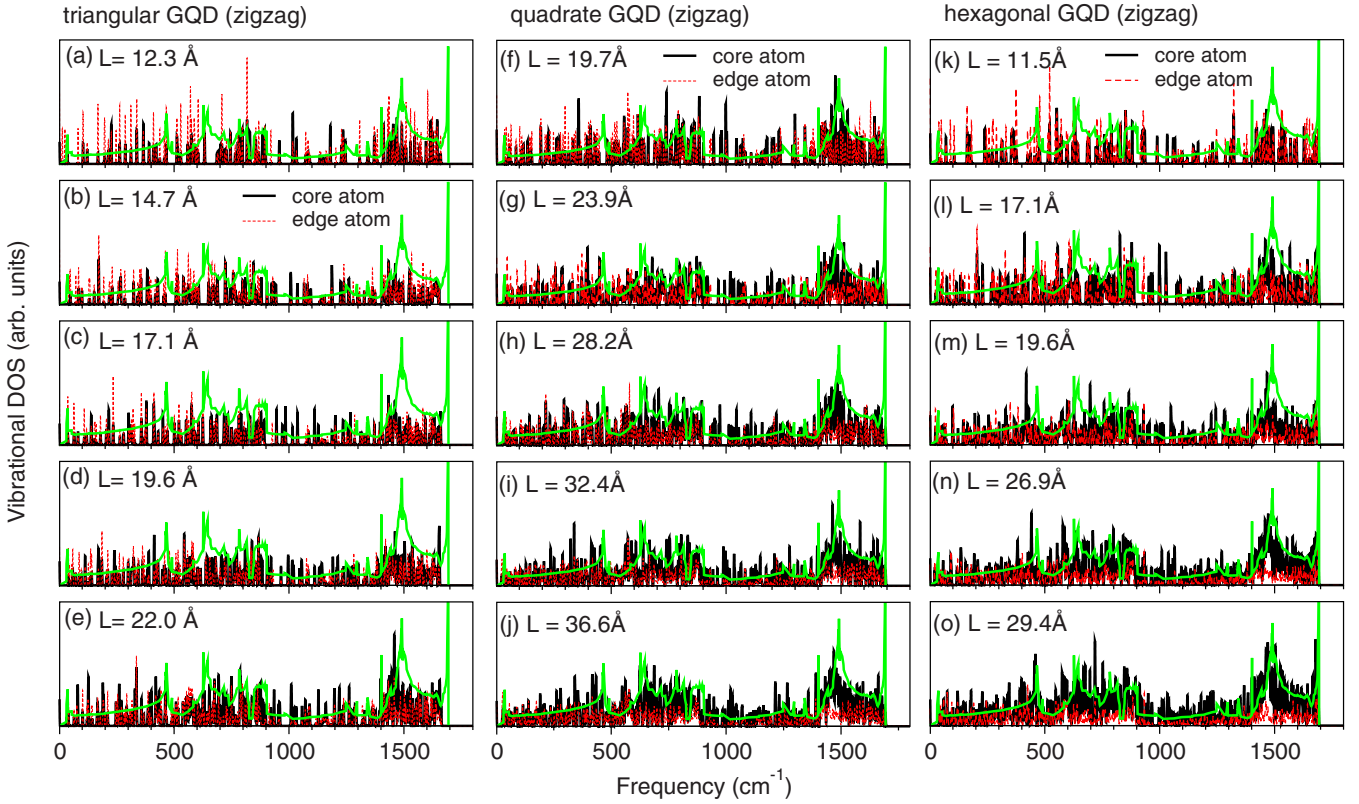


FIG. 2. Vibrational DOS contributed by the motion of core atoms (solid black lines) and edge atoms (dashed red lines) of [(a)–(e)] triangular GQDs, [(f)–(j)] quadrate GQDs, and [(k)–(o)] hexagonal GQDs with zigzag edge structure. Phonon DOS of SLG is plotted as solid green lines.

vector \mathbf{q} . The vibrational eigenvectors $\mathbf{u}_{n,\mathbf{q}}$ along with the phonon dispersion of SLG are calculated via *ab initio* density functional perturbation theory (DFPT) implemented in the Quantum ESPRESSO code [41,42] using the same pseudopotentials and the same energy cutoff as those for GQDs. A Monkhorst-Pack k -point mesh of $18 \times 18 \times 1$ is used in the DFPT calculation.

III. VIBRATIONAL DENSITY OF STATES

Before investigating the vibrational properties of GQDs, we start our discussion from the phonon states of pristine SLG. In Figs. 1(b) and 1(c), we present our calculated phonon dispersion curve of SLG along $\Gamma \rightarrow M \rightarrow K \rightarrow \Gamma$ direction with the phonon DOS. As shown in Fig. 1(b), frequency of the out-of-plane vibrated acoustic (ZA) mode of SLG is lower than that of the in-plane transverse and longitudinal acoustic (TA, LA) modes. Vibrational frequencies of the out-of-plane and in-plane optical modes display an analogous relation to those of the acoustic modes. Due to the lack of acoustic-optic phonon band gap, we see an overlap between the frequencies of the out-of-plane optical (ZO) mode and the LA mode within the frequency range of 800–1000 cm^{-1} around the M point of the Brillouin zone (BZ). Moreover, a q^2 -dependent dispersion of ZA mode around the BZ center is obtained as a consequence of the point group symmetry [43,44].

After looking at the phonon properties of SLG, we now focus on the lattice vibrations of GQDs. Figures 2(a)–2(o) shows the calculated vibrational DOS of triangular, quadrate and hexagonal GQDs with zigzag edge structure and differ-

ent sizes. In this figure, lattice vibrations contributed by the motion of the core and edge atoms are color-coded as solid black and dashed red lines, respectively. To benchmark the vibrational DOS of GQDs with SLG, we plot the calculated phonon DOS of SLG as solid green lines. Both the vibrational DOS of GQDs and SLG are plotted with a broadening of 0.8 cm^{-1} . From Fig. 2, we see higher vibrational DOS located within the frequency region below 400 cm^{-1} and the range between 900 to 1400 cm^{-1} for GQDs compared to SLG, especially for small dots. As indicated in Fig. 1(b) and 1(c), these frequency regions are highly overlapped with the frequencies of ZA and ZO modes of SLG, respectively. Moreover, the maxima in the phonon DOS of SLG located around 450 cm^{-1} , 650 cm^{-1} , and 1500 cm^{-1} , which correspond to the van Hove singularities of the acoustic and optical branches, disappear in the vibrational DOS of GQDs with small sizes. These results indicate that the out-of-plane vibrations instead of in-plane modes dominate the lattice vibrations of small GQDs. Later, we will see these out-of-plane modes are not the analogues of ZA/ZO modes but the transverse standing waves induced by lateral confinement via projecting the vibrational eigenmodes of GQDs on SLG. (See Supplemental Material for the movies of the confined acoustic modes of GQD [45].) In contrast, we find high density of vibrational modes locates around 550 cm^{-1} , which is between two van Hove singularities of SLG (located at 450 cm^{-1} and 650 cm^{-1}) for GQDs with different sizes and shapes. These modes are identified as a series of in-plane vibrated acoustic modes. The movies of these modes are provided within the Supplemental Material [45].

Following the discussion on the vibrational DOS of zigzag edged GQDs, we now turn to GQDs with armchair edges. Contrast to edges along the zigzag orientation, where non-bonding π -electron state exists in the edge region, the local state disappears in armchair edges [46,47]. We therefore study the lattice vibrations of armchair edged GQDs without hydrogen passivation. In Figs. 3(a)–3(k), we present the calculated vibrational DOS of armchair edged GQDs with triangular [(a)–(d)], quadrate [(e)–(g)], and hexagonal [(h)–(k)] structures. In this figure, vibrations contributed by the motion of the core and the edge atoms are plotted as solid-black and dashed-red lines with solid-green lines for the phonon DOS of SLG. Similar to GQDs with zigzag edges, we find the out-of-plane vibrated confinement modes play an important role on the lattice vibrations of armchair edged GQDs with small sizes. Moreover, high density of in-plane vibrated acoustic phonon modes also appears in the calculated vibrational DOS with frequency around 550 cm^{-1} . Comparing to zigzag edged GQDs, we see the density of the in-plane vibrated optical modes with frequency around 1500 cm^{-1} , which corresponds to the van Hove singularity of the LO and TO branches of SLG (dominated by the vibrations of LO and TO phonons with wave vectors located between M to K points and around K point in the direct of $K \rightarrow \Gamma$ in the reciprocal space), is relatively weaker in armchair edged GQDs. Instead, high density of vibrational modes with optical characters display a red shift to the frequency range between 1400 and 1500 cm^{-1} in armchair edged GQDs. To reveal the red shift of the optical-like modes in armchair edged GQDs, we turn to look at the bond lengths of GQDs with the same geometry shapes but different edge structures. As shown in Figs. 2 and 3, these high-density optical modes are mainly contributed by the vibration of core atoms, especially for large dots. We thus calculate the average bond length of the core atoms in GQDs. For the largest GQDs we studied in, the average bond length of core atoms \bar{a}_c of triangular GQD with zigzag edges is 1.412 \AA , while that of the armchair edged triangular GQD is 1.417 \AA . Similar to triangular GQD, the values of \bar{a}_c of quadrate (hexagonal) GQDs with zigzag and armchair edge structures are 1.411 \AA (1.409 \AA) and 1.416 \AA (1.417 \AA), respectively. Due to the positive Grüneisen parameters of the LO and TO phonon modes of graphene [48], the longer average bond length of armchair edged GQDs leads to the lower frequency of the optical-like modes.

As shown in Figs. 2 and 3, the vibrational DOS of GQDs displays a tendency to mimic that of SLG as the size of the GQD increases. In order to quantitatively analyze such tendency, we define a similarity function as

$$S_{\text{VDOS}} = \sum_n \frac{f_{\text{VDOS}}^{\text{GQD}}(\omega_n) f_{\text{VDOS}}^{\text{SLG}}(\omega_n)}{|f_{\text{VDOS}}^{\text{SLG}}(\omega_n)|^2}, \quad (4)$$

where $f_{\text{VDOS}}^{\text{GQD(SLG)}}(\omega_n)$ is the normalized vibrational DOS of GQD (SLG) with $|f_{\text{VDOS}}^{\text{GQD(SLG)}}(\omega_n)|^2 = 1$, and ω_n denotes the frequency of the n th grid of the vibrational DOS. The calculated similarity function S_{VDOS} of GQDs with triangular (black circles), quadrate (red squares), and hexagonal (green triangles) shapes are presented in Figs. 4(a) and 4(b) for

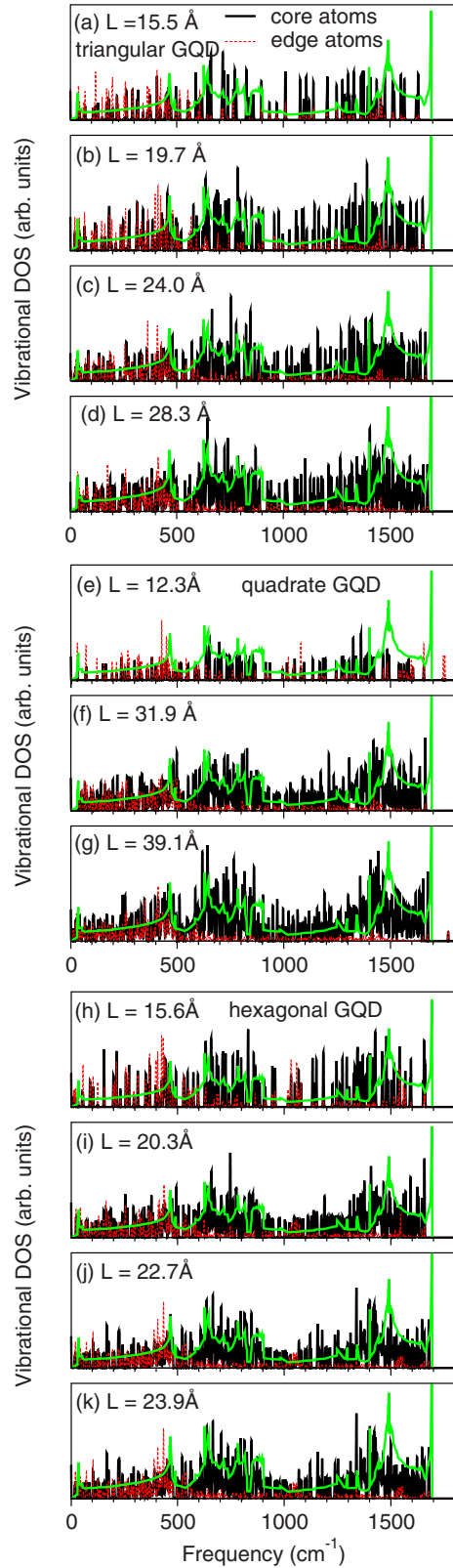


FIG. 3. Vibrational DOS contributed by the motion of core atoms (solid-black lines) and edge atoms (dashed-red lines) of (a)–(d) triangular GQDs, (e)–(g) quadrate GQDs, and (h)–(k) hexagonal GQDs with armchair edge structure. Phonon DOS of SLG is given as solid-green lines.

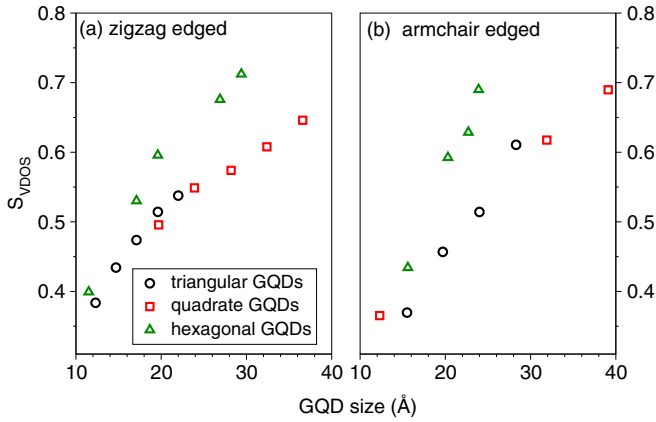


FIG. 4. Size dependence of the similarity function S_{VDOS} of triangular (black circles), quadrate (red squares), and hexagonal (green triangles) shaped GQDs with (a) zigzag and (b) armchair edge structures.

zigzag and armchair edge structures, respectively. As shown in Fig. 4, we find the similarity value S_{VDOS} of hexagonal GQDs increases from 0.4 to more than 0.7 with dot size L increasing from 12 Å to 29 Å for the case of zigzag edges and increases from 0.45 to 0.7 for the armchair edged ones with L increasing from 16 Å to 24 Å. Similarly, the S_{VDOS} value of triangular (quadrate) GQDs with zigzag edges increases from less than 0.4 (0.5) to around 0.55 (0.65) when the dot size increases from 12 Å to 22 Å (from 20 Å to 36 Å), while the S_{VDOS} value increases from more than 0.35 to around 0.6 (0.7) when the dot size of armchair edged triangular (quadrate) GQDs increases from 16 Å to 28 Å (from 12 Å to 39 Å). In addition, we notice that the slope of S_{VDOS} of GQDs with hexagonal shape is higher than that of GQDs with other geometry structures. We attribute the high similarity between vibrations of hexagonal shaped GQDs and SLG to their point group symmetry, i.e., both of them have D_{6h} point group symmetry.

In order to investigate the origin of the lattice vibrations of GQDs, we proceed to quantitatively analyze the parentage of SLG phonon mode via projecting the vibrational eigenvectors of GQD on those of SLG as indicated in Eq. (3). In Figs. 5(a)–5(f), we present the square of the calculated projection coefficient $|C_n^v|^2 = \sum_{q \in BZ} |C_{n,q}^v|^2$ of triangular, quadrate, and hexagonal GQDs with both zigzag and armchair edge structures on the ZA (black lines), TA (red lines), LA (green lines), ZO (blue lines), TO (violet lines), and LO (cyan lines) modes of SLG along with the corresponding vibrational DOS. Comparing Fig. 5 with Figs. 1(b) and 1(c), we find the following features of the lattice vibrations of GQDs. First of all, only a few GQD modes keep the vibrational character of SLG. Contrast to the in-plane (LA and TA) and out-of-plane (ZA) acoustic modes of SLG, the lateral confinement of GQDs combining the propagating wave with various wave vector \mathbf{q} into standing waves via reflections at the boundary. (See Supplemental Material for the movies of the confined acoustic modes of GQD [45].) Due to the large values of edge-area ratio in small GQDs, the out-of-plane vibrated standing waves dominate the acoustic vibrations of small GQDs. Moreover, we notice that lateral confinement mixes

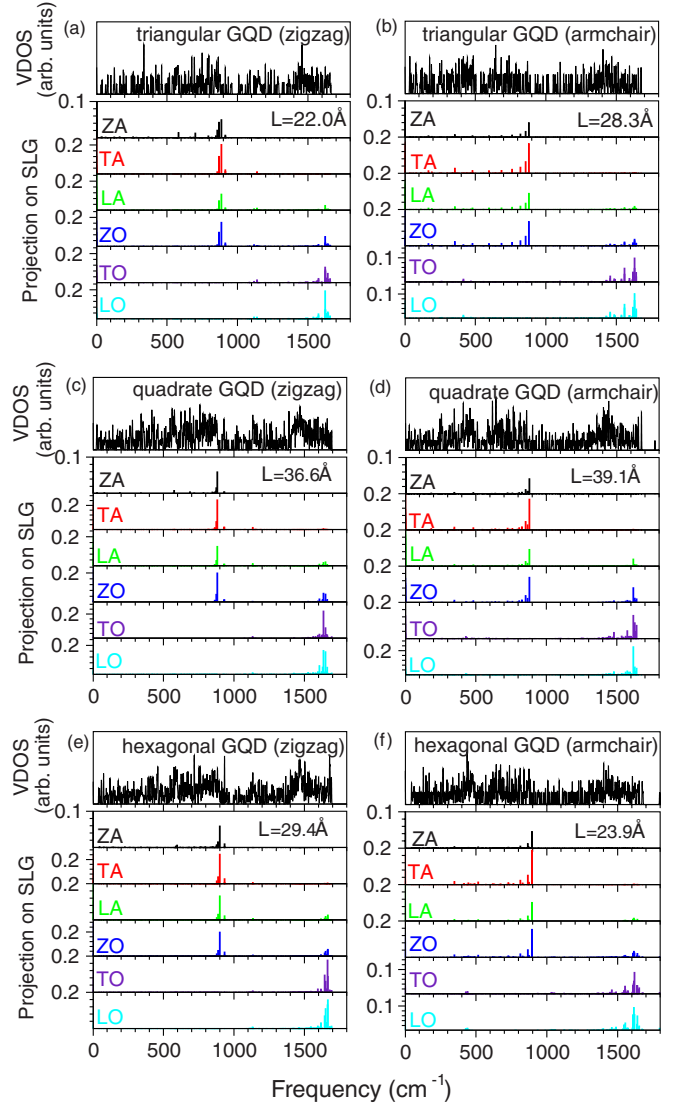


FIG. 5. Vibrational DOS along with the projection coefficient of GQD vibrational modes on the ZA (black lines), TA (red lines), LA (green lines), ZO (blue lines), TO (violet lines), and LO (cyan lines) phonon modes of SLG for (a) zigzag edged triangular GQD with $L = 22.0$ Å, (b) armchair edged triangular GQD with $L = 28.3$ Å, (c) zigzag edged quadrate GQD with $L = 36.6$ Å, (d) armchair edged quadrate GQD with $L = 39.1$ Å, (e) zigzag edged hexagonal GQD with $L = 29.4$ Å, and (f) armchair edged hexagonal GQD with $L = 23.9$ Å.

the in-plane longitudinal and transverse characters with the characters of out-of-plane vibrations for both acoustic and optical modes of GQDs. This leads to the appearance of ZA, TA, and LA characters in GQD modes with frequency around 900 cm⁻¹, which is higher than that of the ZA and TA modes of SLG. Similar to acoustic modes, the optical modes of GQDs with frequencies around 1650 cm⁻¹ display both the in-plane optical and the ZO mode parentage even though the highest frequency of the ZO mode is lower than 1400 cm⁻¹. In contrast to the confined modes with mixed vibrational characters, we see obvious ZO and LO/TO phonon characters in the vibrations of GQDs with frequencies of 880 cm⁻¹ and

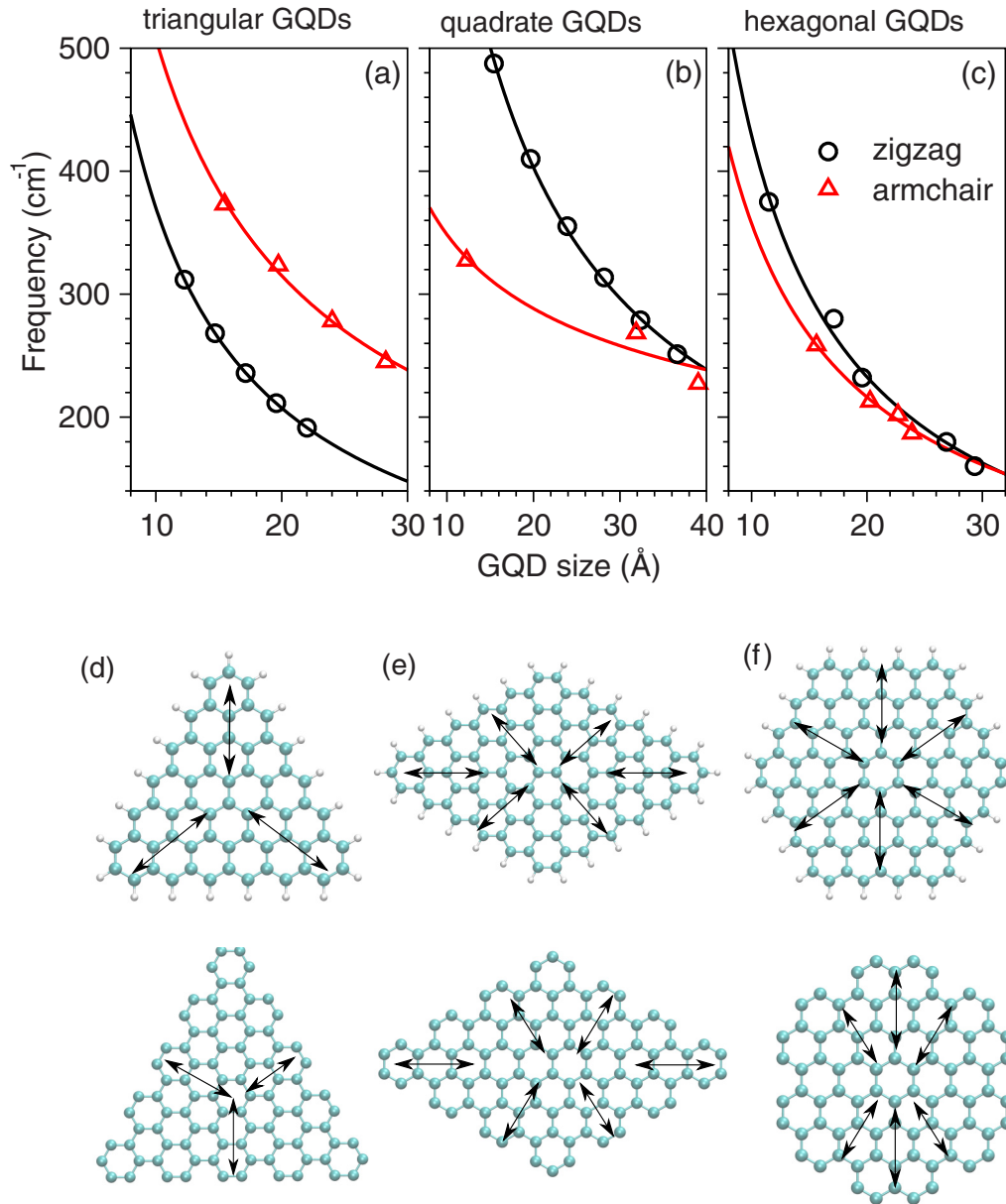


FIG. 6. Lowest coherent acoustic phonon modes of (a) triangular, (b) quadrate, and (c) hexagonal GQDs with zigzag (black triangles) and armchair (red circles) edges obtained from *ab initio* calculation. Size dependence of lowest coherent acoustic modes fitted by $\omega_c = \alpha L^{-\beta}$ for zigzag and armchair edged GQDs are given as solid black and red lines, respectively. Schematic illustration of motions of the coherent acoustic modes of GQDs with zigzag (top column) and armchair (bottom column) edges for dots with (d) triangular, (e) quadrate, and (f) hexagonal shapes.

1650 cm⁻¹, which correspond to the ZO and LO/TO phonon frequencies of SLG in the center of the BZ.

Comparing the properties of the acoustic and optical phonon modes of GQDs, we see stronger lateral confinement on acoustic modes than optical ones. We attribute the significant changes of acoustic modes with lateral confinement to the characters of the motion of atoms in these modes. In the case of acoustic phonon modes, the displacements of two carbon atoms in the unit cell are in the same direction and the vibrations of acoustic modes can be viewed as elastic waves [36,49]. The mechanical boundary conditions lead to the existing of many confined acoustic modes as a series of standing waves in GQDs. Unlike acoustic modes, optical

phonon modes do not involve a macroscopic strain of the material. Instead, two carbon atoms in the unit cell move in opposite direction. Such relative displacements of charged atoms generate a macroscopic electric field. Thus, both mechanical and electric boundary conditions are required for optical modes. This results in the formation of surface optical phonon modes and a few confined optical phonon modes in GQDs. (See Supplemental Material for the details [45].) In addition to the different confinement effects on acoustic and optical modes, we observe a higher LO/TO phonon parentage of SLG in zigzag edged GQDs than the one with armchair edges. This result indicates a strong confinement effect on lattice vibrations of GQDs edged with armchair orientation.

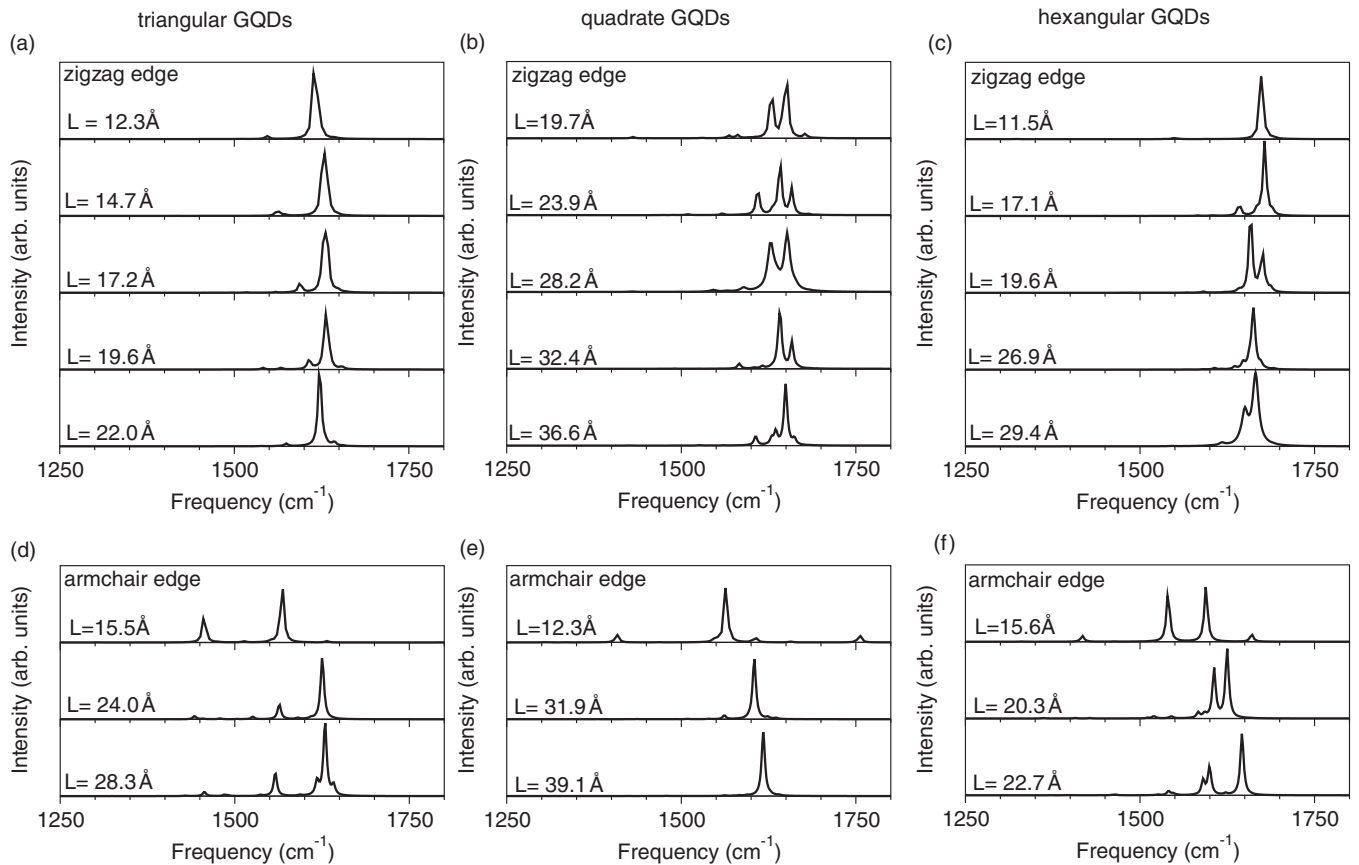


FIG. 7. Calculated Raman spectra of GQDs for difference sizes with triangular, quadrate and hexagonal shapes and zigzag and armchair edges.

IV. COHERENT ACOUSTIC MODES

Following the discussion on the vibrational DOS, we now turn to the coherent acoustic phonon mode in GQDs, which is an important type of vibrations in low-dimensional nanostructures with both Raman and far-infrared activity [37]. In the coherent acoustic phonon mode, all the atoms in GQDs vibrate in phase as a motion of breathing and this mode is also named as breathing mode. (See Supplemental Material for the videos of coherent acoustic modes of GQDs with different geometry and edge structures [45].) The frequencies of the lowest coherent acoustic modes of GQDs with triangular, quadrate, and hexagonal shapes are presented as a function of dot size L in Fig. 6(a)–6(c). In this figure, phonon frequencies obtained from DFT calculations are plotted as black triangles and red circles for GQDs with zigzag and armchair edges, respectively. Corresponding fitting curves $\omega_c = \alpha L^{-\beta}$ for the zigzag and armchair edged GQDs are given as solid black and red lines, respectively. Fitting parameters α and β of GQDs with different geometry and edge structures are listed in the Supplemental Material [45]. As shown in Table I within the Supplemental Material, the value of β for zigzag edged GQDs increases from 0.76 (with quadrate shape) to 0.84 (with triangular shape) and to 0.88 (with hexagonal shape) while those of the corresponding armchair edged GQDs are 0.27, 0.69, and 0.72, respectively. Comparing to GQDs with triangular, quadrate, and hexagonal shapes, the size dependence of the vibrational frequency of coherent acoustic phonon of

spherical QDs was described by $\omega_c = \eta R^{-1}$ with parameter η and the radius of the spherical dot R [50,51]. This result indicates that the value of β , which corresponds to the size dependence of coherent acoustic phonon frequency, increases with increasing the isotropy of nanostructure.

As shown in Figs. 6(a)–6(c), we find the following features of the coherent acoustic phonon modes of GQDs. First of all, as a kind of confinement mode, the vibrational frequency of the coherent acoustic phonon decreases with increasing dot size. Secondly, the frequency of the coherent acoustic mode in GQDs with zigzag edges is higher than that with armchair edges for the case of quadrate and hexagonal structures. In contrast, the coherent acoustic modes of triangular dots with zigzag edges vibrate more slowly than those of the armchair edged analogues. To understand the different size dependence of coherent acoustic phonon frequency, we present the schematic illustration of the motion of atoms of the coherent acoustic phonon mode in GQDs as black arrows in Figs. 6(d)–6(f). From Figs. 6(d)–6(f), we see various confinement on the lattice vibrations along zigzag and armchair edge orientations. Due to different geometry structures, the directions of the coherent acoustic vibrations are similar for GQDs with zigzag and armchair edges in the case of quadrate or hexagonal structure. In contrast, the vibration direction of the coherent acoustic mode is much different for triangular GQDs with zigzag and armchair edges. As a result, stronger confinement in the armchair orientation leads to the higher

frequency of coherent acoustic mode in the corresponding triangular GQDs. Moreover, we see from Fig. 6 that the frequencies of the coherent acoustic mode of quadrate GQDs are higher than those of triangular and hexagonal dots with similar sizes. This is the result of strong confinement between edges induced by their anisotropy geometry structure.

V. RAMAN INTENSITY

In addition to the coherent acoustic mode, another type of important vibrational mode in GQDs is the Raman-active mode. As a unique and powerful experimental technique, Raman spectroscopy has been widely used to study the vibrational properties of graphene [25,27,29,52,53]. In layered graphene with large dimension and high quality, two strong peaks named as G-mode and 2D-mode, which correspond to the in-plane vibrated optical mode and a two phonon lattice vibrational process are presented in the measured Raman spectrum [52]. To investigate the effect of lateral confinement on the G-mode position in the Raman spectra of GQDs, we calculate the Raman intensity of GQDs via the empirical model proposed by Richter *et al.* [54]:

$$I(\omega) \propto \sum_{n,v,q} \frac{|C_{n,q}^v|^2}{(\omega - \omega^v)^2 + (\Gamma_0/2)^2}, \quad (5)$$

with the projection coefficient $C_{n,q}^v$ obtained from Eq. (3) and the vibrational frequency of GQDs ω^v . In our calculation, the natural Lorentzian linewidth Γ_0 is taken as 10 cm^{-1} and the coefficients $C_{n,q}^v$ are summed up to $\Delta q \approx 1/L$. As indicated in the previous research, the G-mode of SLG with zigzag-dominated edges is determined by the vibration of TO mode while only LO mode is active at the armchair-dominated edges [29,55]. We therefore calculate the Raman spectra of zigzag and armchair edged GQDs via Eq. (5) by summing the projection on the TO and LO modes, respectively.

In Fig. 7, we show the calculated Raman spectra of zigzag and armchair edged GQDs with triangular [(a) and (d)], quadrate [(b) and (e)] and hexagonal [(c) and (f)] shapes for different sizes. From this figure, we see the peak positions of the G-mode in the zigzag edged GQDs are around 1650 cm^{-1} while those of the armchair edged ones locate in the frequency range between 1550 to 1650 cm^{-1} . Both of them are higher than that of SLG, which is around 1585 cm^{-1} [25,29]. Moreover, we observe a red shift of the G-mode position in large GQDs with zigzag edges. Since the vibrational frequency of the TO- and LO-like modes is highly sensitive to the bond length of materials, we turn to the bond lengths of GQDs to understand the features of the G-mode positions. In Fig. 8(a)–8(f), we plot the bond lengths, i.e., the nearest-neighbor distances between carbon atoms, of the relaxed GQDs as a function of the distance between the bond center to the dot center. As shown in Fig. 8, the bond length around the dot center is around 1.41 \AA , which is very close to that of SLG, for all cases. In the case of GQDs with hydrogen terminated zigzag edges [shown in Figs. 8(a)–8(c)], the bond lengths reduce to around 1.38 \AA at the dot edges with 2.1% reduction. In contrast, the bond lengths at the edges of GQDs with armchair edge orientation [shown in Figs. 8(d)–8(f)] are around 1.30 \AA with a reduction of 7.8%. We explain the decrease

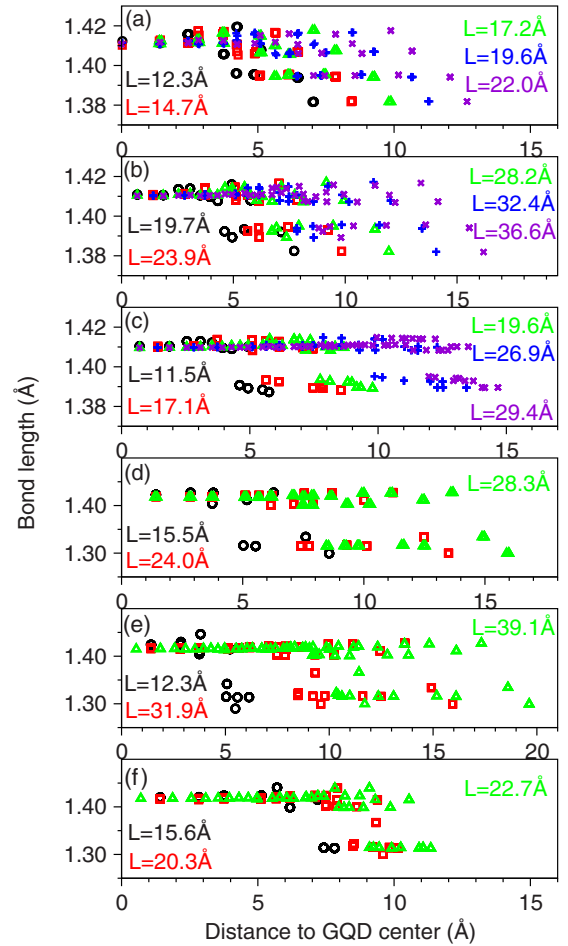


FIG. 8. Bond-length distribution as a function of their distance to the GQD center for (a) triangular GQDs with zigzag edges, (b) quadrate GQDs with zigzag edges, (c) hexagonal GQDs with zigzag edges, (d) triangular GQDs with armchair edges, (e) quadrate GQDs with armchair edges, and (f) hexagonal GQDs with armchair edges.

of the bond length at the dot edges as the result of surface effect for all cases and attribute the large reduction of bond length at armchair edges to the lack of surface passivation. Owing to the reduction of bond lengths at the dot edges along with the positive Grüneisen parameters of LO and TO modes in graphene [48], a blue shift of the G-mode is obtained in GQDs. As shown in Fig. 8, we find a high percentage of short length bonds in large GQDs with armchair edges. This leads to the blue shift of the G-mode position in armchair edged GQDs with increasing dot size. Combining Fig. 7 with 8, we notice that the G-mode positions of zigzag and armchair edged GQDs are close to each other, even though large difference between bond lengths at the edges with different orientations. We attribute the similar blue shift of GQDs with zigzag and armchair edges to their different contributions from the motion of edge atoms on the Raman active modes. As shown in Figs. 2 and 3, the motion of edge atoms play a more important role on the vibration of G-mode in zigzag edged GQDs than the armchair edged ones.

VI. SUMMARY

In summary, we study the vibrational properties of triangular, quadrangle, and hexagonal shaped GQDs with both zigzag and armchair edge structures for different sizes via *ab initio* DFT calculations. We show that the vibrational DOS of GQDs changes from a molecular type discrete-like form to a form of SLG phonon DOS with increasing dot size. In addition to the confinement effect, the feature of the vibrational DOS also depends on the point group symmetry of GQDs. We find that the out-of-plane vibrated standing waves induced by lateral confinement instead of the in-plane modes dominate the vibrations of GQDs with small sizes. By projecting the vibrational eigenvectors of GQDs on those of SLG, we see only a few modes of GQDs keep the parentage of SLG phonon modes, and the strong lateral confinement leads to the mixture of the in-plane and out-of-plane vibration characters. We find stronger confinement on the vibrations of acoustic modes than optical modes from both *ab initio* calculation and continuum

model analysis. We also identify the coherent acoustic phonon modes of GQDs and find different confinement effects in the zigzag and armchair orientations. Moreover, stronger size dependence of coherent acoustic phonon frequency is obtained in nanostructures with higher isotropy. We further calculate the Raman intensity of GQDs with different sizes, shapes and edges. A blue shift of the G-mode position is obtained in GQDs compared to SLG, and this blue shift is attributed to the results of surface effect.

ACKNOWLEDGMENTS

P.H. acknowledges financial support by the National Natural Science Foundation of China under Grant No. 11774243, Capacity Building for Science & Technology Innovation–Fundamental Scientific Research Funds (008/19530050170 and 008/19530050180). The work was carried out at National Supercomputer Center in Tianjin, and the calculations were performed on TianHe-1 (A).

-
- [1] K. S. Novoselov, A. K. Geim, S. V. Morozov, D. Jiang, Y. Zhang, S. V. Dubonos, I. V. Grigorieva, and A. A. Firsov, Electric field effect in atomically thin carbon films, *Science* **306**, 666 (2004).
- [2] A. K. Geim and K. S. Novoselov, The rise of graphene, *Nat. Mater.* **6**, 183 (2007).
- [3] K. S. Novoselov, V. I. Fal'ko, L. Colombo, P. R. Gellert, M. G. Schwab, and K. Kim, A roadmap for graphene, *Nature (London)* **490**, 192 (2012).
- [4] F. Bonaccorso, Z. Sun, T. Hasan, and A. C. Ferrari, Graphene photonics and optoelectronics, *Nat. Photonics* **4**, 611 (2010).
- [5] F. Schwierz, Graphene transistors, *Nat. Nanotech.* **5**, 487 (2010).
- [6] A. A. Balandin, Thermal properties of graphene and nanostructured carbon materials, *Nat. Mater.* **10**, 569 (2011).
- [7] A. H. Castro Neto, F. Guinea, N. M. R. Peres, K. S. Novoselov, and A. K. Geim, The electronic properties of graphene, *Rev. Mod. Phys.* **81**, 109 (2009).
- [8] M. Liu, X. B. Yin, E. Ulin-Avila, B. S. Geng, T. Zentgraf, L. Ju, F. Wang, and X. Zhang, A graphene-based broadband optical modulator, *Nature (London)* **474**, 64 (2011).
- [9] Q. Bao and K. P. Loh, Graphene photonics, plasmonics, and broadband optoelectronic devices, *ACS Nano* **6**, 3677 (2012).
- [10] D. Pan, J. Zhang, Z. Li, and M. Wu, Hydrothermal route for cutting graphene sheets into blue-luminescent graphene quantum dots, *Adv. Mater.* **22**, 734 (2010).
- [11] X. T. Zheng, A. Ananthanarayanan, K. Q. Luo, and P. Chen, Glowing graphene quantum dots and carbon dots: Properties, syntheses, and biological applications, *Small* **11**, 1620 (2015).
- [12] D. Walkup, F. Ghahari, C. Gutiérrez, K. Watanabe, T. Taniguchi, N. B. Zhitenev, and J. A. Stroscio, Tuning single-electron charging and interactions between compressible Landau level islands in graphene, *Phys. Rev. B* **101**, 035428 (2020).
- [13] Z.-Q. Fu, Y. Pan, J.-J. Zhou, K.-K. Bai, D.-L. Ma, Y. Zhang, J.-B. Qiao, H. Jiang, H. Liu, and L. He, Relativistic artificial molecules realized by two coupled graphene quantum dots, *Nano Lett.* **20**, 6738 (2020).
- [14] V. Gupta, N. Chaudhary, R. Srivastava, G. D. Sharma, R. Bhardwaj, and S. Chand, Luminescent graphene quantum dots for organic photovoltaic devices, *J. Am. Chem. Soc.* **133**, 9960 (2011).
- [15] W. Kwon, Y.-H. Kim, C.-L. Lee, M. Lee, H. C. Choi, T.-W. Lee, and S.-W. Rhee, Electroluminescence from graphene quantum dots prepared by amidative cutting of tattered graphite, *Nano Lett.* **14**, 1306 (2014).
- [16] Q. Zhang, J. Jie, S. Diao, Z. Shao, Q. Zhang, L. Wang, W. Deng, W. Hu, H. Xia, X. Yuan, and S.-T. Lee, Solution-processed graphene quantum dot deep-UV photodetectors, *ACS Nano* **9**, 1561 (2015).
- [17] X. Li, M. Rui, J. Song, Z. Shen, and H. Zeng, Carbon and graphene quantum dots for optoelectronic and energy devices: A review, *Adv. Funct. Mater.* **25**, 4929 (2015).
- [18] A. Xu, G. Wang, Y. Li, H. Dong, S. Yang, P. He, and G. Ding, Carbon-based quantum dots with solid-state photoluminescent: Mechanism, implementation, and application, *Small* **16**, 2004621 (2020).
- [19] W.-S. Kuo, X.-C. Shen, C.-Y. Chang, H.-F. Kao, S.-H. Lin, J.-Y. Wang, and P.-C. Wu, Multiplexed graphene quantum dots with excitation-wavelength-independent photoluminescence, as two-photon probes, and in ultraviolet-near infrared bioimaging, *ACS Nano* **14**, 11502 (2020).
- [20] J. Lee, D. Wong, J. Velasco Jr., J. F. Rodriguez-Nieva, S. Kahn, H.-Z. Tsai, T. Taniguchi, K. Watanabe, A. Zettl, F. Wang, L. S. Levitov, and M. F. Crommie, Imaging electrostatically confined Dirac fermions in graphene quantum dots, *Nat. Phys.* **12**, 1032 (2016).
- [21] C. Gutierrez, L. Brown, C.-J. Kim, J. Park, and A. N. Pasupathy, Klein tunnelling and electron trapping in nanometre-scale graphene quantum dots, *Nat. Phys.* **12**, 1069 (2016).
- [22] M. Zarenia, A. Chaves, G. A. Farias, and F. M. Peeters, Energy levels of triangular and hexagonal graphene quantum dots: A comparative study between the tight-binding and Dirac equation approach, *Phys. Rev. B* **84**, 245403 (2011).

- [23] J. Milton Pereira, P. Vasilopoulos, and F. M. Peeters, Tunable quantum dots in bilayer graphene, *Nano Lett.* **7**, 946 (2007).
- [24] P. E. Allain and J. N. Fuchs, Klein tunneling in graphene: Optics with massless electrons, *Eur. Phys. J. B* **83**, 301 (2011).
- [25] A. C. Ferrari, J. C. Meyer, V. Scardaci, C. Casiraghi, M. Lazzeri, F. Mauri, S. Piscanec, D. Jiang, K. S. Novoselov, S. Roth, and A. K. Geim, Raman Spectrum of Graphene and Graphene Layers, *Phys. Rev. Lett.* **97**, 187401 (2006).
- [26] Z. H. Ni, H. M. Wang, J. Kasim, H. M. Fan, T. Yu, Y. H. Wu, Y. P. Feng, and Z. X. Shen, Graphene thickness determination using reflection and contrast spectroscopy, *Nano Lett.* **7**, 2758 (2007).
- [27] D. L. Mafra, G. Samsonidze, L. M. Malard, D. C. Elias, J. C. Brant, F. Plentz, E. S. Alves, and M. A. Pimenta, Determination of LA and TO phonon dispersion relations of graphene near the Dirac point by double resonance raman scattering, *Phys. Rev. B* **76**, 233407 (2007).
- [28] T. M. G. Mohiuddin, A. Lombardo, R. R. Nair, A. Bonetti, G. Savini, R. Jalil, N. Bonini, D. M. Basko, C. Galiotis, N. Marzari, K. S. Novoselov, A. K. Geim, and A. C. Ferrari, Uniaxial strain in graphene by raman spectroscopy: *G* peak splitting, grüneisen parameters, and sample orientation, *Phys. Rev. B* **79**, 205433 (2009).
- [29] C. Cong, T. Yu, and H. Wang, Raman study on the *G* mode of graphene for determination of edge orientation, *ACS Nano* **4**, 3175 (2010).
- [30] M. L. Mueller, X. Yan, B. Dragnea, and L.-S. Li, Slow hot-carrier relaxation in colloidal graphene quantum dots, *Nano Lett.* **11**, 56 (2011).
- [31] J. P. Trinastic, I.-H. Chu, and H.-P. Cheng, Manipulating the phonon bottleneck in graphene quantum dots: Phonon-induced carrier relaxation within the linear response theory, *J. Phys. Chem. C* **119**, 22357 (2015).
- [32] S. Reichardt and C. Stampfer, Modeling charge relaxation in graphene quantum dots induced by electron-phonon interaction, *Phys. Rev. B* **93**, 245423 (2016).
- [33] M. A. Darehdor, M. R. Roknabadi, and N. Shahtahmassebi, Effects of phonon scattering on the electron transport and photocurrent of graphene quantum dot structures, *Eur. Phys. J. B* **92**, 10 (2019).
- [34] J. Wu, W. Pisula, and K. Müllen, Graphenes as potential material for electronics, *Chem. Rev.* **107**, 718 (2007).
- [35] X. Yan, X. Cui, and L.-S. Li, Synthesis of large, stable colloidal graphene quantum dots with tunable size, *J. Am. Chem. Soc.* **132**, 5944 (2010).
- [36] P. Y. Yu and M. Cardona, In *Fundamentals of Semiconductors* (Springer, Berlin, 2010).
- [37] P. Han and G. Bester, Confinement effects on the vibrational properties of III-V and II-VI nanoclusters, *Phys. Rev. B* **85**, 041306(R) (2012).
- [38] P. Han and G. Bester, Insights about the surface of colloidal nanoclusters from their vibrational and thermodynamic properties, *J. Phys. Chem. C* **116**, 10790 (2012).
- [39] CPMD, <http://www.cpmd.org/>, Copyright jointly by IBM Corp. and Max Planck Institute, Stuttgart.
- [40] P. Han and G. Bester, Heavy strain conditions in colloidal core-shell quantum dots and their consequences on the vibrational properties from *ab initio* calculations, *Phys. Rev. B* **92**, 125438 (2015).
- [41] P. Giannozzi, S. Baroni, N. Bonini, M. Calandra, R. Car, C. Cavazzoni, D. Ceresoli, G. L. Chiarotti, M. Cococcioni, I. Dabo *et al.*, QUANTUM ESPRESSO: A modular and open-source software project for quantum simulations of materials, *J. Phys.: Condens. Matter.* **21**, 395502 (2009).
- [42] P. Giannozzi, O. Andreussi, T. Brumme, O. Bunau, M. B. Nardelli, M. Calandra, R. Car, C. Cavazzoni, D. Ceresoli, M. Cococcioni *et al.*, Advanced capabilities for materials modelling with QUANTUM ESPRESSO, *J. Phys.: Condens. Matter.* **29**, 465901 (2017).
- [43] R. Saito, G. Dresselhaus, and M. S. Dresselhaus, *Physical Properties of Carbon Nanotubes*, (Imperial College, London, 1998).
- [44] D. L. Nika and A. A. Balandin, Phonons and thermal transport in graphene and graphene-based materials, *Rep. Prog. Phys.* **80**, 036502 (2017).
- [45] See Supplemental Material at <http://link.aps.org/supplemental/10.1103/PhysRevB.104.085430> for details on the fitting parameters of size dependence of coherent acoustic phonon frequency, the derivation of confined acoustic and optical phonon modes in a confined system, and the videos of the vibrational modes.
- [46] S. E. Stein and R. L. Brown, π -electron properties of large condensed polyaromatic hydrocarbons, *J. Am. Chem. Soc.* **109**, 3721 (1987).
- [47] Y. Kobayashi, K.-I. Fukui, T. Enoki, K. Kusakabe, and Y. Kaburagi, Observation of zigzag and armchair edges of graphite using scanning tunneling microscopy and spectroscopy, *Phys. Rev. B* **71**, 193406 (2005).
- [48] Y. C. Cheng, Z. Y. Zhu, G. S. Huang, and U. Schwingenschlögl, Grüneisen parameter of the *G* mode of strained monolayer graphene, *Phys. Rev. B* **83**, 115449 (2011).
- [49] L. D. Landau and E. M. Lifshitz, *Theory of Elasticity, 2nd ed.* (Pergamon Press, Oxford, 1970).
- [50] A. Tanaka, S. Onari, and T. Arai, Low-frequency Raman scattering from CdS microcrystals embedded in a germanium dioxide glass matrix, *Phys. Rev. B* **47**, 1237 (1993).
- [51] T. Huang, P. Han, X. Wang, S. Feng, W. Sun, J. Ye, and Y. Zhang, Theoretical study on ultrafast dynamics of coherent acoustic phonons in semiconductor nanocrystals, *J. Phys. D: Appl. Phys.* **49**, 185101 (2016).
- [52] C. Thomsen and S. Reich, Double Resonant Raman Scattering in Graphite, *Phys. Rev. Lett.* **85**, 5214 (2000).
- [53] A. C. Ferrari and D. M. Basko, Raman spectroscopy as a versatile tool for studying the properties of graphene, *Nat. Nanotech.* **8**, 235 (2013).
- [54] H. Richter, Z. P. Wang, and L. Ley, The one phonon Raman-spectrum in microcrystalline silicon, *Solid State Commun.* **39**, 625 (1981).
- [55] K. Sasaki, R. Saito, K. Wakabayashi, and T. Enoki, Identifying the orientation of edge of graphene using *G* band Raman spectra, *J. Phys. Soc. Jpn.* **79**, 044603 (2010).